# Weak localization of biexcitons in quantum wells

O. Mayrock, H.-J. Wünsche, and F. Henneberger
*Humboldt-Universität zu Berlin, Institut für Physik, Invalidenstrasse 110, D-10117 Berlin, Germany*

C. Riva, V. A. Schweigert,* and F. M. Peeters
*Departement Natuurkunde, Universiteit Antwerpen (UIA), Universiteitsplein 1, B-2610 Antwerpen, Belgium*
(Received 17 December 1998)

Recent experimental studies have demonstrated localization of biexcitons in quantum wells, providing even optical gain up to elevated temperatures. We present a theoretical treatment of exciton and biexciton states in the weak localization limit using a center-of-mass separation ansatz. An advanced approach based on an extensive numerical solution is compared with a more simple model for the quantum well biexciton wave function. Our explicit results, derived for parameters of the ternary quantum well material (Zn,Cd)Se, yield that the localization of the biexciton is—despite its larger spatial extension—stronger than that of the single exciton state. [S0163-1829(99)07031-9]

## I. INTRODUCTION

Localization of excitons induced by disorder (interface roughness, alloy fluctuations, etc.) is an inherent feature of quantum wells (QWs).[1] Recently, various experimental groups[2–4] have reported on the observation of localized biexcitons, providing even optical gain up to elevated temperatures.[4] A common feature of these investigations is that the biexciton binding energy, taken from the separation of the biexciton and exciton photoluminescence (PL) lines, is substantially increased through the localization.[5] It is tempting to relate this finding with calculations for strictly zero-dimensional biexcitons in quantum dots with infinite barriers.[6] In the present case, however, the potential fluctuations are on the same scale as the biexciton binding energy, making a straightforward prediction about the change of the biexciton state under localization impossible. A first calculation in the framework of the density functional theory in local-density approximation indicated that the localized biexciton is approximately twice as stable as the localized exciton.[3,7] A general uncertainty of the local-density approximation is that it produces an artificial self-localization even when the external potential is removed. In the present paper, we present therefore a more elaborated treatment of the biexciton in the limit of weak localization avoiding this artifact.

Our approach is based on the assumption that localization of both the exciton and biexciton can be treated in terms of the center-of-mass (c.m.) motion. This ansatz, so far used for the exciton only,[8] requires knowledge of the biexciton internal wave function for the ideal QW, for which we developed two models. The more precise approach is made by discretizing the Schrödinger equation in real space and solving it with a combination of the inverse iteration technique and a modification of the Gauss-Seidel method.[9] To have an alternative with clearly less numerical expenditure, we make an adiabatic-like hole-hole separation ansatz based on the two-dimensional (2D) hydrogen molecule,[10] extended towards finite hole masses and a finite well width. In the numerical calculations we use parameters appropriate to (Zn,Cd)Se/ZnSe QW structures, characterized by large biexciton binding energies of the order of 10 meV.

The paper is organized as follows. Section II introduces the formalism of the c.m. separation ansatz for the biexciton wave function and the general procedure used in the subsequent sections. The models for the QW biexciton relative wave function and the corresponding treatments of the exciton are the subject of Sec. III. The results are presented and discussed in Sec. IV, where a comparison and an assessment of the two models is made.

## II. GENERAL TREATMENT

In the QWs under consideration, the subband energy separation is much larger than both binding and localization energy of the respective complex, justifying a separation of the single-particle motion in growth direction (in the following denoted as $z$ direction):

$$\Psi_{3D}=\Psi_{2D}\prod_a \varphi_a(z_a), \tag{1}$$

where $a$ runs over all particles ($e,h$ for the exciton and $e1,e2,h1,h2$ for the biexciton) and $\varphi_a(z_a)$ are the single-particle subband functions. The resulting in-plane effective mass Schrödinger equation for the exciton and biexciton reads as

$$\sum_a \left[ -\frac{\hbar}{2m_a}\Delta_{\mathbf{r}_a}+V_a(\mathbf{r}_a)+\sum_{b\neq a}\tilde{U}_{ab}\right]\Psi_{2D} = \left(E-\sum_a E_a^z\right)\Psi_{2D}, \tag{2}$$

which includes the single-particle localization potentials $V_a$ and the effective 2D QW Coulomb interaction potentials

 

$$\tilde{U}_{ab}(\mathbf{r}_a-\mathbf{r}_b)=\int dz_a dz_b \varphi_a^2(z_a)\varphi_b^2(z_b) \times\frac{q_a \quad q_b}{4\pi\varepsilon_o\varepsilon\sqrt{(\mathbf{r}_a-\mathbf{r}_b)^2+(z_a-z_b)^2}}, \quad (3)$$

with the in-plane coordinate $\mathbf{r}_i$ and the charge $q_i$ of particle $i=e,h$ and the dielectric constant $\varepsilon$. The total energy and the single-particle QW confinement energies are denoted as $E$ and $E_a^z$, respectively.

In the limit of weak localization, the internal motion of the complex is almost not affected. Therefore, we can solve the problem of the internal motion and the c.m. problem separately by making the ansatz

$$\Psi_{2D}=\psi(\mathbf{R})\phi(\{\mathbf{q}\}), \quad (4)$$

where $\phi$ is the wave function of the internal motion, depending on an appropriate set of relative in-plane coordinates $\{\mathbf{q}\}$, and solving

$$\left[T_{\mathrm{rel}}+\sum_{a,b}\tilde{U}_{ab}\right]\phi(\{\mathbf{q}\})=E_{\mathrm{rel}}\phi(\{\mathbf{q}\}), \quad (5)$$

with $T_{\mathrm{rel}}$ the kinetic energy operator and $E_{\mathrm{rel}}$ the energy defining the binding energy of the complex in the ideal QW. $\psi$ and $\mathbf{R}$ are the c.m. wave function and coordinate, respectively. Inserting ansatz (4) into the Schrödinger equation (2), multiplying with $\phi^*$ and integrating with respect to the relative coordinates yields the c.m. Schrödinger equation

$$[T_{\mathrm{c.m.}}+V_{\mathrm{c.m.}}(\mathbf{R})]\psi(\mathbf{R})=-E_{\mathrm{loc}}\psi(\mathbf{R}), \quad (6)$$

where $T_{\mathrm{c.m.}}$ and $E_{\mathrm{loc}}=\Sigma_a E_a^z+E_{\mathrm{rel}}-E$ denote the kinetic energy operator and the localization energy of the c.m. motion, respectively. The c.m. potential

$$V_{\mathrm{c.m.}}(\mathbf{R})=\sum_a \int d^2s F_a(s)V_a(\mathbf{R}+\mathbf{s}) \quad (7)$$

can be expressed as a sum over convolution integrals of the single-particle localization potential $V_a$ with a weight function

$$F_a(s)=\int d\{\mathbf{q}\}\phi^2(\{\mathbf{q}\})\delta(\mathbf{r}_a(\mathbf{R},\{\mathbf{q}\})-\mathbf{R}-\mathbf{s}) \quad (8)$$

for each particle $a$. They are normalized by the normalization of the wave function $\phi$. Here, $\mathbf{r}_a(\mathbf{R},\{\mathbf{q}\})$ are the individual coordinates of the particle $a$ in terms of the c.m. and relative coordinates. Concluding so far, the localization energy $E_{\mathrm{loc}}$ can be calculated directly from the simple effective single-particle equation (6), if the weight functions $F_a(s)$—which are functions of only one variable $s$, the distance from the c.m.—for the electrons and holes in the free excitonic complex in the QW are known.

In case of the single exciton, the relative wave function $\phi$ has the only coordinate $\mathbf{q}=\mathbf{r}_e-\mathbf{r}_h$, so that $\mathbf{r}_a=\mathbf{R}\pm(\mu/m_a)\mathbf{q}$ with the reduced exciton mass $\mu=m_e m_h/(m_e+m_h)$. Consequently, the weight functions are simply[8,11]

$$F_a(s)=\phi^2\left(\frac{m_a}{\mu}s\right) \quad (a=e,h). \quad (9)$$

In the next section, we introduce two models for the biexciton relative wave function in the ideal QW.

## III. THE QUANTUM WELL BIEXCITON WEIGHT FUNCTION

### A. Numerical solution of the finite-difference biexciton Schrödinger equation

Schweigert *et al.*[9] have developed a numerical method for calculating the ground state of an interacting many-particle system. Instead of solving the Schrödinger equation by a diagonalization of the Hamiltonian using an expansion of the wave function in a basis consisting of product eigenfunctions of the single-particle Hamiltonian, the method of Ref. 9 solves directly the Hamiltonian of a finite system of interacting particles confined by a given potential. In the many-body Schrödinger equation we use a finite-difference representation of the Laplacian for $k$ degrees of freedom on a space grid with $n$ points. This leads to a large $n^k\times n^k$ sparse matrix. The number of nonzero elements of the matrix is proportional to $n^k$. The present procedure requires $n^k$ operations to find the ground state, which allow us to consider systems with $k=4$–6 degrees of freedom on non-parallel machines. It should be noted, that recently considerable attention has been paid to construct effective algorithms to solve the many-body Schrödinger equation using mean field theoretical approximations for the exchange correlation energy (see, e.g., Ref. 12 for a brief review). In particular the finite-difference technique was considered for an effective one-particle problem.[13] To solve the problem of the biexciton in an ideal QW,[9] the finite-difference technique was extended in order to solve the many-particle Schrödinger equation. The effective 2D Coulomb potential is approximated by[14,15]

$$\tilde{U}_{ab}(\mathbf{r}_a-\mathbf{r}_b)\approx\frac{q_a q_b}{4\pi\epsilon_o\varepsilon\sqrt{(\mathbf{r}_a-\mathbf{r}_b)^2+(\alpha d_{\mathrm{QW}})^2}}, \quad (10)$$

avoiding the logarithmic singularities of the rigorous expression (3). $\alpha$ is a fitting parameter, which is equal to 0.2 in case of infinitely high QW barriers and which depends on the width $d_{\mathrm{QW}}$ of the QW in case of finite barrier height. Choosing $\alpha$ such that the resulting QW exciton relative wave function approaches the one obtained by using the effective 2D QW Coulomb potential (3) as close as possible, we find $\alpha=0.26$ for a 18 monolayer $Zn_{0.8}Cd_{0.2}Se/ZnSe$ QW

$$[m_e=0.15m_0, \quad m_h=0.5m_0 \ \text{(isotropic)}, \quad \epsilon=8.8,$$

$$Ry=20.3 \ \text{meV}, \quad a_B=4.0 \ \text{nm}, \quad \Delta E_g=260 \ \text{meV},$$

$$\chi_c=\Delta E_c/\Delta E_g=0.75, \quad d_{\mathrm{QW}}=5.2 \ \text{nm}].$$

Standard enumeration of the single exciton equation yields an exciton binding energy of 32.7 meV, being in very good agreement with the value of 32.3 meV for the more accurate potential (3). Both potentials as well as exciton wave functions are plotted for comparison in Fig. 1. Solving next the biexciton equation within the above mentioned numerical scheme, we obtain a biexciton binding energy of 3.81 meV

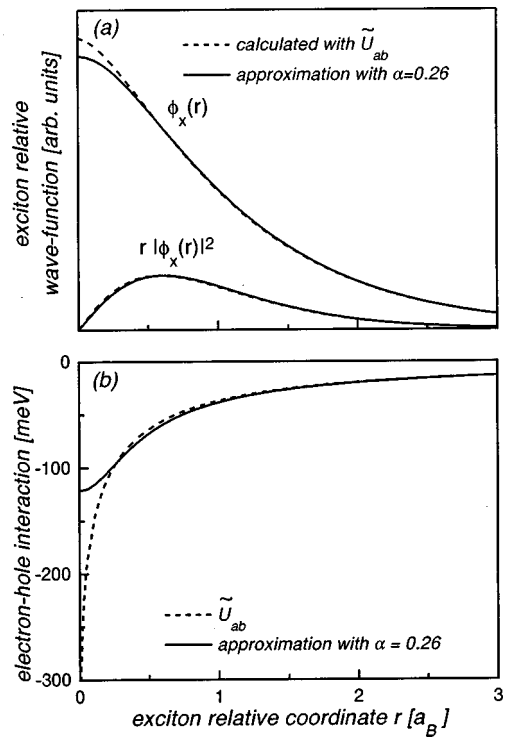


FIG. 1. Exciton relative wave functions and probability densities (a), and effective 2D QW Coulomb potentials (b) in an 18 monolayer (5.2 nm) $Zn_{0.8}Cd_{0.2}Se/ZnSe$ QW. Dotted line: potential $\tilde{U}_{ab}$, given by Eq. (3). Solid line: approximation for $\tilde{U}_{ab}$, given by Eq. (10) with $\alpha=0.26$.

for the ideal QW. This value is about three times smaller than experimental data,[3,4] emphasizing the role of localization in real QW structures.

The respective weight functions $F_a(s)$ for electrons and holes in the exciton and the biexciton are shown in Fig. 2. For the exciton, the hole weight function is stronger located at the c.m. compared to the electron weight function because of the larger hole mass. As known for the protons in the hydrogen molecule, the hole weight function in the biexciton displays instead a local minimum at the c.m., caused by the Coulomb repulsion of the holes together with their smaller

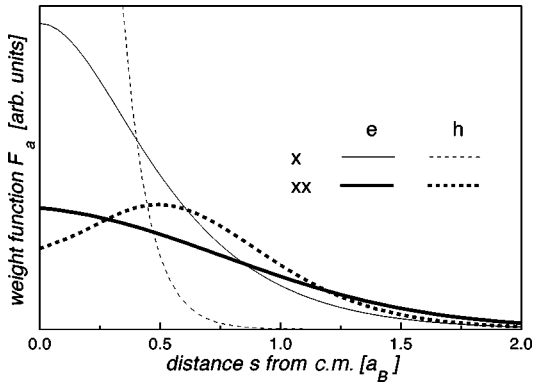


FIG. 2. Normalized weight functions $F_a(s)$ $(a=e,h)$ for the exciton and the biexciton. The results for the biexciton (thick curves) are obtained by numerically solving the finite-difference Schrödinger equation. As for the biexciton, the results for the exciton (thin curves) are calculated using Eq. (10) with $\alpha=0.26$.

kinetic energy compared to the electrons. The maximum of the electron probability density lies between the holes in the c.m., screening the hole-hole repulsion and making the binding of the complex possible.

### B. Hole-hole separation ansatz

To have an alternative approach with clearly less numerical expenditure, we tried to find a supplementary, more simple model for the QW biexciton relative wave function. An effective one-degree-of-freedom model,[16] which ignores relevant kinetic energy terms, yielded very poor results, even qualitatively different from those of the previous section. Therefore, we developed another approximation for the QW biexciton wave function which is based on an adiabaticlike hole-hole separation ansatz, outlined in the following.

In the limit of large hole mass $(\sigma=m_e/m_h\ll 1)$, a decoupling

$$\phi(\{\mathbf{q}\})=\phi_A(\{\mathbf{q}\})\cdot\Phi(h) \tag{11}$$

is well suited for constructing an in-plane biexciton relative wave function, where $h$ denotes the hole-hole distance. An appropriate choice for the internal wave function is the variational ansatz

$$\phi_A=\frac{\phi_x(\gamma r_{e1h1})\phi_x(\gamma r_{e2h2})+\phi_x(\gamma r_{e1h2})\phi_x(\gamma r_{e2h1})}{\sqrt{2(1+S^2)}}, \tag{12}$$

where $\phi_x$ is the exciton relative wave function, depending on the electron-hole distance $r_{ab}$ $(a=e1,e2;\quad b=h1,h2)$, $S$ is the overlap integral, and $\gamma$ is a variational parameter accounting for a compression of the exciton within the biexciton. This provides the Schrödinger equation

$$\left[-\frac{\hbar^2}{M}\left(\frac{\partial^2}{\partial h^2}+\frac{1}{h}\frac{\partial}{\partial h}\right)+V(h)\right]\Phi(h)=E_{xx}\Phi(h) \tag{13}$$

for the factor $\Phi(h)$, where $M=m_e+m_h$ is the exciton total mass. For the sake of simplicity, instead of calculating the effective exciton-exciton potential $V(h)$ with the aid of Eq. (12) by extensive numerical efforts, we approximate this potential by

$$V(h)=V_M(h)+\frac{e^2}{4\pi\varepsilon_o\varepsilon h}e^{-h/b}, \tag{14}$$

with the Morse potential[17] $V_M(h)=D\cdot[(1-e^{-a(h-h_o)})^2-1]$. The second term ensures the correct asymptotic behavior for $h\to 0$, which consists of a screened Coulomb repulsion of the holes. For finding the parameters $D$, $h_o$, $a$, and $b$ in a QW, an interpolation between the potentials of the hydrogen molecule in 2D (Ref. 10) and 3D (Ref. 18) is made. Since the mass $M$ may be considered as infinite in this case, binding energy and hole-hole separation are directly given by the minimum of the potential curve. The respective parameters are summarized in Table I. For a better comparison of the two potential curves, both plotted in Fig. 3, we rescale the space and energy coordinates in 2D and 3D by the respective exciton radius (most probable electron-hole distance) $\rho_d(d=2\mathrm{D},3\mathrm{D})$ and exciton binding energy $E_x^{b(d)}$,

TABLE I. Exciton binding energy $E_x^{b(d)}$, exciton radius (most probable electron-hole distance) $\rho_d$, compression parameter $\gamma$, and the fitting parameters $D, h_o, a, b$ for the potential (14) for 2D, 3D and for an 18 monolayer (5.2 nm) $Zn_{0.8}Cd_{0.2}Se/ZnSe$ QW.

| $d$ | $E_x^{b(d)}$ [Ry] | $\rho_d$ [$a_B$] | $\gamma$ | $D$ [Ry] | $h_o[a_B]$ | $a[a_B^{-1}]$ | $b[a_B]$ |
|---|---|---|---|---|---|---|---|
| 2D | 4.0 | 0.25 | 1.275 | 2.45 | 0.35 | 2.7 | 0.09 |
| 3D | 1.0 | 1.0 | 1.166 | 0.35 | 1.45 | 1.15 | 0.09 |
| QW | 1.57 | 0.54 | 1.227 | linear combination according to Eq. (16) | | | |

also listed in Table I. Though the absolute values are markedly different, the minima of the resulting rescaled potentials

$$U_d(h/\rho_d) = V_d(h)/E_x^{b(d)} \tag{15}$$

appear nearly at the same position $h/\rho_d \approx 1.4$ (see inset of Fig. 3), indicating that the size of the molecule scales with the size of the atoms. Hence, it seems reasonable to assume that the same scaling rule holds for the QW. We use a linear interpolation between the 2D and 3D potential

$$U_{\mathrm{QW}}(x) = \xi U_{\mathrm{2D}}(x) + (1-\xi) U_{\mathrm{3D}}(x), \tag{16}$$

with $x = h/\rho_{\mathrm{QW}}$ and the interpolation parameter $\xi = (\rho_{\mathrm{QW}} - \rho_{\mathrm{3D}})/(\rho_{\mathrm{2D}} - \rho_{\mathrm{3D}})$, where $\rho_{\mathrm{QW}}$ is derived from the exciton wavefunction solving potential (3). The resulting potential $V_{\mathrm{QW}}(h)$ is plotted in Fig. 3 together with the probability density $|\Phi(h)|^2$, obtained from the solution of the hole-hole Schrödinger equation (13). It should be noted, that the choice for $\xi$ is somewhat arbitrary, but other reasonable interpolations yielded only slightly different results in our numerical examples.

The calculation of the weight functions $F_a(s)$ additionally requires knowledge of the compression parameter $\gamma$ in Eq. (12). For this purpose, we interpolate in the same way like for the potential $U_{\mathrm{QW}}$ between the two values for 2D (Ref. 10) and for 3D (Ref. 19), listed in Table I. Using an exponential trial function for $\phi_x$, we find for the 18 monolayer $Zn_{0.8}Cd_{0.2}Se/ZnSe$ QW the values $E_x^{b(\mathrm{QW})} = 31.6$ meV $= 1.57$ Ry, $\rho_{\mathrm{QW}} = 2.2$ nm $= 0.54 a_B$, $\gamma = 1.23$, and a biexciton binding energy $E_{xx}^b = 2E_x - E_{xx} = 4.68$ meV with $\xi = 0.61$.

The derivation of the weight functions $F_a(s)$ (labeled as B in Fig. 4), from the adiabatic-like biexciton wave function (11) is outlined in the appendix. We find very good agreement between models A and B, concerning the qualitative behavior of the weight functions as well as the spatial extension of the complex. The hole weight function of the hole-hole separation ansatz shows a sharper peak at equilibrium position and a smaller value for $s = 0$ than that of the finite-difference calculation. The latter might be caused by the different asymptotic behavior of the particle-particle potentials for vanishing distance. Equation (10) underestimates the hole-hole repulsion by avoiding a singularity, whereas the screened $1/h$ potential in Eq. (14) diverges stronger than the logarithmic divergency of the true QW Coulomb potential. Despite of the various simplifications within this hole-hole separation ansatz, the results agree surprisingly well with the

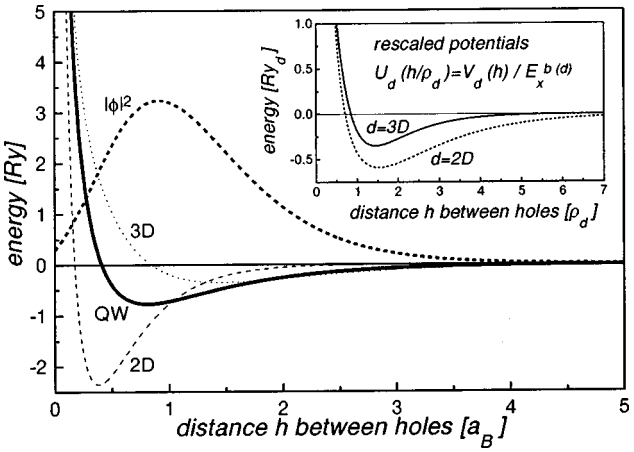


FIG. 3. Effective exciton-exciton interaction potentials $V(h)$. Thin dotted line: 3D. Thin dashed line: 2D. Thick solid line: interpolation for an 18 monolayer (5.2 nm) $Zn_{0.8}Cd_{0.2}Se/ZnSe$ QW. Thick dashed line: probability distribution $|\Phi(h)|^2$ for the QW case. Inset: Rescaled potentials $U_d(h/\rho_d)$ for the 2D and 3D cases.

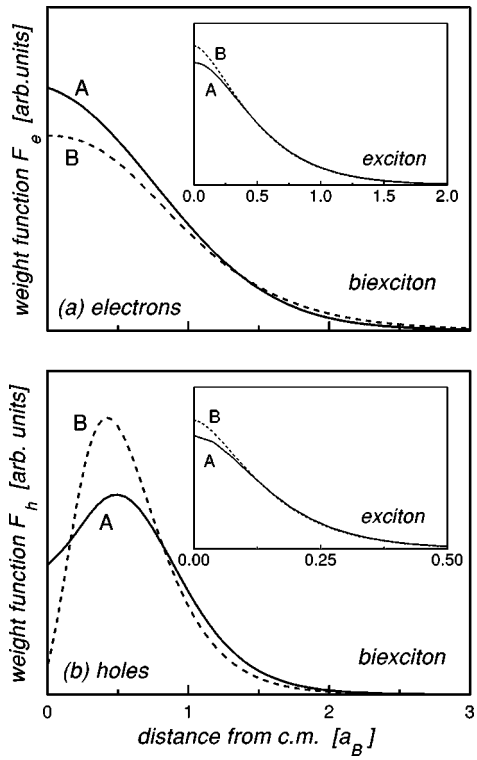


FIG. 4. Normalized weight functions $F_a(s)$ $(a = e,h)$ for the two models of the QW biexciton relative wave function. *A*: Numerical solution of the finite-difference Schrödinger equation. *B*: Hole-hole separation ansatz. Insets: Weight functions for the electron and the hole in the respective exciton.

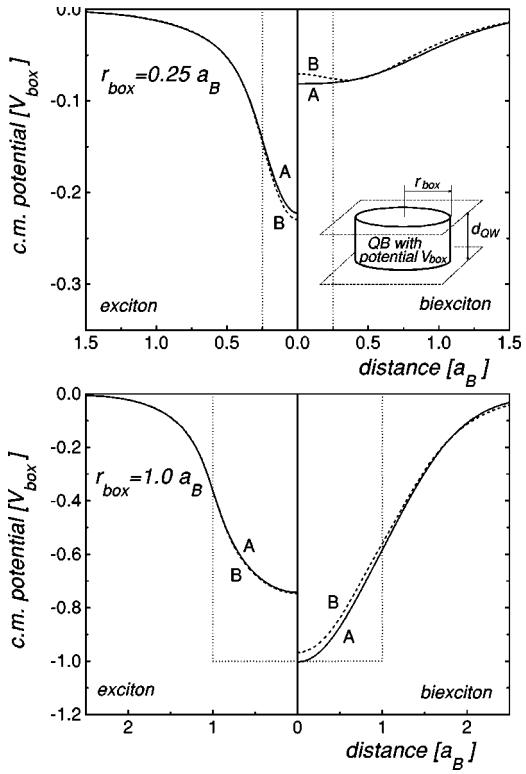


FIG. 5. Center-of-mass potentials $V_{\mathrm{c.m.}}$ of the exciton (left side) and the biexciton (right side) for two QB radii $r_{\mathrm{box}}^{(1)}=0.25a_B$ (upper layer) and $r_{\mathrm{box}}^{(2)}=1.0a_B$ (lower layer) for the two biexciton models: *A*: Numerical solution of the finite-difference Schrödinger equation. *B*: Hole-hole separation ansatz. Dotted line: The single-particle localization potentials $V_a$.

advanced numerical solution of the finite-difference Schrödinger equation, introduced in Sec. III A.

## IV. LOCALIZATION ENERGIES

The exciton and biexciton localization is considered for cylindrical one-particle potentials

$$V_a(\mathbf{r}_a)=\begin{cases}\chi_a V_{\mathrm{box}} & \begin{cases}\text{if} \quad r_a\leqslant r_{\mathrm{box}}\\ \text{and} \quad -\dfrac{d_{\mathrm{QW}}}{2}<z<\dfrac{d_{\mathrm{QW}}}{2}\end{cases}\\ 0 & \text{else}\end{cases} \tag{17}$$

of variable radius $r_{\mathrm{box}}$ and potential depth $V_{\mathrm{box}}$, covering the full QW-width $d_{\mathrm{QW}}$ in $z$ direction (see inset of Fig. 5).[20,21] This kind of quantum box (QB) represents an accumulation of material with smaller band gap, surrounded by material with larger band gap. The coefficient $\chi_a=\Delta E_a/\Delta E_g$ denotes the relative conduction and valence band offset, respectively. As the localization potential (17) is axial-symmetric, the c.m. Schrödinger equation (6) is reduced to a one-dimensional problem, which is solved numerically. For the discretization of the radial part of the 2D Laplacian, we use the second-order representation[22]

$$(\Delta\psi)_i=\frac{1}{\delta^2}\left(\frac{R_{i-1/2}}{R_i}\psi_{i-1}-2\psi_i+\frac{R_{i+1/2}}{R_i}\psi_{i+1}\right) \tag{18a}$$

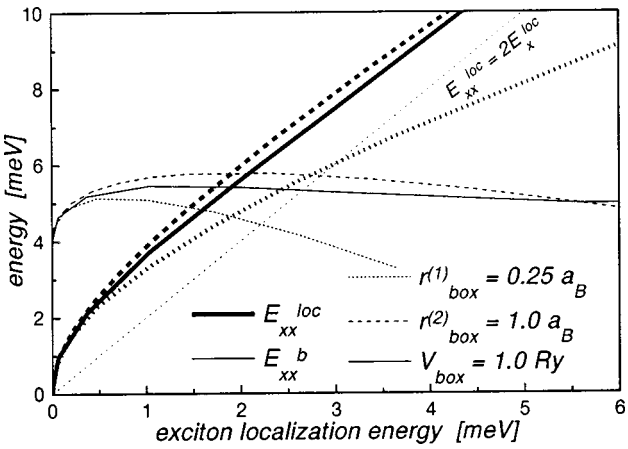


FIG. 6. Biexciton localization and binding energies $E_{xx}^{\mathrm{loc}}$ and $E_{xx}^{b}$ as a function of the exciton localization energy $E_x^{\mathrm{loc}}$ in a QB, embedded in an 18 monolayer (5.2 nm) $Zn_{0.8}Cd_{0.2}Se/ZnSe$ QW. Dotted line: Fixed radius $r_{\mathrm{box}}^{(1)}=0.25a_B$ and variable potential depth $V_{\mathrm{box}}$. Dashed line: Fixed radius $r_{\mathrm{box}}^{(2)}=1.0a_B$ and variable $V_{\mathrm{box}}$. Solid line: Fixed potential depth $V_{\mathrm{box}}=1$ Ry and variable $r_{\mathrm{box}}$. The line with $E_{xx}^{\mathrm{loc}}=2E_x^{\mathrm{loc}}$ marks the case of equal localization strength per exciton.

and

$$(\Delta\psi)_0=\frac{4}{\delta^2}(\psi_1-\psi_0) \tag{18b}$$

for $i\neq 0$ and $i=0$, respectively. $R_i$ is the c.m. coordinate on the numerical grid point $i$, and $\delta=R_{i+1}-R_i$ is the increment of the grid. Our explicit calculations are again carried out for a 18 monolayer $Zn_{0.8}Cd_{0.2}Se/ZnSe$ QW.

### A. Increased biexciton localization

We start discussing the results obtained with the QW biexciton relative wave function calculated by solving the finite-difference Schrödinger equation (Sec. III A). The respective c.m. potentials $V_{\mathrm{c.m.}}$ for two QB radii $r_{\mathrm{box}}^{(1)}=0.25a_B$ and $r_{\mathrm{box}}^{(2)}=1.0a_B$ are depicted in Fig. 5 (solid curves, labeled with A). While the shape of the potential curve is independent of the depth $V_{\mathrm{box}}$ of the single-particle potential $V_a$, the ground-state energy levels $E_x^{\mathrm{loc}}$ and $E_{xx}^{\mathrm{loc}}$ as well as their position relative to each other depend sensitively on this parameter.

Conversely to the model parameters $r_{\mathrm{box}}$ and $V_{\mathrm{box}}$, the exciton localization energy $E_x^{\mathrm{loc}}$ is a quantity directly observable experimentally. Therefore, we chose this energy, calculated at the respective level of approximations, as reference for measuring the degree of the biexciton localization. In Fig. 6, biexciton localization and binding energies $E_{xx}^{\mathrm{loc}}$ and $E_{xx}^{\mathrm{b}}=2E_x-E_{xx}$, respectively, are plotted versus $E_x^{\mathrm{loc}}$, varying the parameters of the QB in two ways. First, variation of $V_{\mathrm{box}}$ at the selected radii $r_{\mathrm{box}}^{(1)}$ and $r_{\mathrm{box}}^{(2)}$ demonstrates how the biexciton localizes when its spatial extension is approximately equal or distinctly smaller than the characteristic width of $V_{\mathrm{c.m.}}$ (dashed curves). Second, keeping the potential depth $V_{\mathrm{box}}=1.0$ Ry fixed, the radius $r_{\mathrm{box}}$ was varied (solid curves). As long as the localization is weak, the biexciton is found to have a larger localization energy per exciton than

the single exciton, despite its larger spatial extension. (For small exciton localization energies, the biexciton localization energies lie above the line with $E_{xx}^{\mathrm{loc}}=2E_{x}^{\mathrm{loc}}$ in Fig. 6.) In our definition, the biexciton binding energy represents in fact the separation of the exciton and biexciton PL features. Decomposing the various contributions, it holds $E_{xx}^{b}=E_{xx}^{b\ \mathrm{ideal}}+(E_{xx}^{\mathrm{loc}}-2E_{x}^{\mathrm{loc}})$, where $E_{xx}^{b\ \mathrm{ideal}}$ is the binding energy of the ideal QW. The increased line separation in the experiment is hence a consequence of the stronger biexciton localization, while the exciton-exciton interaction energy remains practically unchanged.

This fact can also be understood as an increased biexciton binding energy compared to the free QW biexciton, for which the solution of the finite-difference Schrödinger equation yields $E_{xx}^{b}=3.81$ meV.

The asymptotic behavior for $E_{x}^{\mathrm{loc}}\rightarrow 0$ can be shown to be universal and independent of the details of the potential and the relative wave function: For any particle with mass $M$ localized in a weak 2D potential $U(\mathbf{r})[|U|\ll\hbar^2/(Ma^2)$ where $a^2$ is the area where $U$ is significantly different from zero], it holds[23]

$$|E|\approx\frac{\hbar^2}{Ma^2}\exp\left[-\hbar^2/\left(M\int d^2r|U|\right)\right]. \tag{19}$$

Since the weight functions $F_a(s)$ are normalized, the integral of the biexciton c.m. potential $\int d^2r|U|$ is two times that of the exciton, so that the biexciton has not only twice the mass, but sees twice the potential strength compared to the exciton, resulting in

$$|E_{xx}^{\mathrm{loc}}|\sim|E_{x}^{\mathrm{loc}}|^{1/4}. \tag{20}$$

Beyond this limit, the trends for the biexciton localization are directly related to the respective weight functions. For a given $E_{x}^{\mathrm{loc}}$, the larger width of the biexciton function causes a decrease of $E_{xx}^{\mathrm{loc}}$ when $r_{\mathrm{box}}$ becomes smaller. Increasing $V_{\mathrm{box}}$ at fixed $r_{\mathrm{box}}$, $E_{xx}^{\mathrm{loc}}$ crosses the line $E_{xx}^{\mathrm{loc}}=2E_{x}^{\mathrm{loc}}$ at $V_{\mathrm{box}}=150$ meV ($E_{x}^{\mathrm{loc}}=3.0$ meV) for $r_{\mathrm{box}}^{(1)}=0.25a_B$ and at $V_{\mathrm{box}}=26$ meV ($E_{x}^{\mathrm{loc}}=8.5$ meV) for $r_{\mathrm{box}}^{(2)}=1.0a_B$, respectively, where the enhancement of the biexciton localization disappears. On the other hand, for relatively shallow QBs with $V_{\mathrm{box}}\lesssim 1.0$ Ry, no crossover is found in the range of reasonable values of $r_{\mathrm{box}}$. Evidently, the assertion that localization requires a particle size smaller than the characteristic potential extension, is incorrect.

Strictly speaking, the c.m. approach requires $E_{xx}^{\mathrm{loc}}\ll E_{xx}^{b}$. It can be argued however that even the range $E_{xx}^{\mathrm{loc}}\gtrsim E_{xx}^{b}$ can be covered in very good approximation. In the latter situation, the slight compression of the biexciton relative wave function caused by localization is compensated by the Coulomb repulsion of the equally charged particles so that its net change can be ignored.

### B. Comparison of the biexciton models

Now we evaluate the simplified version of the QW biexciton relative wave function, introduced in Sec. III B, by comparing it with the more rigorous treatment of the previous section. Figure 5 displays the respective exciton and biexciton c.m. potentials $V_{\mathrm{c.m.}}$ for the QB radii $r_{\mathrm{box}}^{(1)}$ and $r_{\mathrm{box}}^{(2)}$.

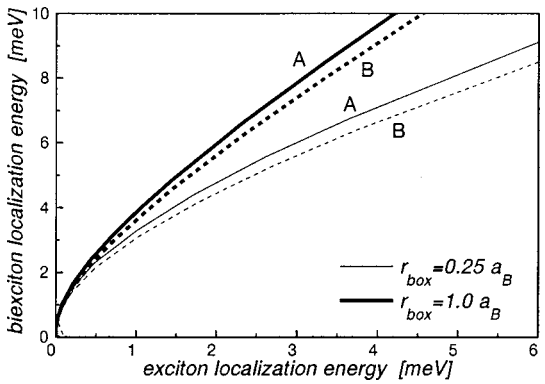


FIG. 7. Biexciton localization energies $E_{xx}^{\mathrm{loc}}$ as functions of the exciton localization energy $E_{x}^{\mathrm{loc}}$ in QBs with $r_{\mathrm{box}}^{(1)}=0.25a_B$ and $r_{\mathrm{box}}^{(2)}=1.0a_B$ for the two biexciton models *A* and *B* (see caption in Fig. 4).

As already demonstrated for the weight functions, the hole-hole separation ansatz reproduces the solution of the finite-difference Schrödinger equation very well. This is also true for the biexciton localization energies $E_{xx}^{\mathrm{loc}}$ plotted versus $E_{x}^{\mathrm{loc}}$ in Fig. 7. A qualitative deviation consists in a nonmonotonic behavior of the potential curve for the narrower QB, caused by the sharper peak of the hole weight function $F_h$ of this approximation. For $\sigma\ll 1$, $V_{\mathrm{c.m.}}$ is controlled by the shape of $F_h$. If the radius of the QB is now smaller than the distance of the hole from the c.m. in the free biexciton, given by the peak of $F_h$, the complex localizes with one hole inside and the other hole outside the QB. While this is indeed the correct scenario for $\sigma\ll 1$, the finite-difference calculation demonstrates that the peak of $F_h$ is less pronounced for the actual $\sigma$, and thus compensated by the contribution of the electron weight function.

## V. CONCLUSION

Our above study has confirmed the localization of biexcitons. In the limit of weak localization, the localization energy is more than twice as large as for the single exciton because of the larger biexciton mass and the stronger c.m. potential. Therefore, with increasing temperature, first the excitons are removed from their localization sites, while localized biexcitons survive up to markedly higher levels. Weak localization of the biexciton significantly increases the biexciton binding energy, given by the separation of the exciton and biexciton PL features, without altering the exciton-exciton interaction energy. Stronger localization, as for instance in intentionally made quantum dots, does not necessarily mean that the stability of the biexciton is further enhanced. For the (Zn,Cd)Se/ZnSe model structure studied here, the Coulomb repulsion of the heavier holes becomes increasingly dominant in the interparticle interaction, so that the biexciton binding energy starts to decrease. This case, where the c.m. approach begins to fail, deserves further investigation. The adiabaticlike hole-hole separation ansatz turned out to provide a useful approximation scheme for calculating the QW biexciton state.

## ACKNOWLEDGMENTS

Part of this work was supported by the Flemish Science Foundation (FWO-Vl) and the ''Interuniversity Poles of At-

traction Program–Belgian State, Prime Minister's Office, Federal Office for Scientific, Technical and Cultural Affairs.'' We also acknowledge the financial support of this work by the Deutsche Forschungsgemeinschaft, and stimulating discussions with R. Zimmermann, E. Runge, and A. Esser.

## APPENDIX: WEIGHT FUNCTIONS OF THE HOLE-HOLE SEPARATION ANSATZ

Here, we outline how to calculate the weight function $F_a(s)$ from the biexciton relative wave function in case of the adiabatic-like hole-hole separation ansatz, introduced in Sec. III B. Using exponential functions for the exciton relative wave function $\phi_x$ in ansatz (11), we obtain for the adiabatic biexciton relative wave function

$$\phi(\mathbf{r}_1,\mathbf{r}_2,\mathbf{h}) = \frac{2}{\pi\sqrt{2(1+S^2)}}\gamma^2(e^{-\gamma r_1}e^{-\gamma r_2} + e^{-\gamma|\mathbf{r}_1-\mathbf{h}|}e^{-\gamma|\mathbf{r}_2+\mathbf{h}|})\Phi(h), \tag{A1}$$

where

$$\mathbf{r}_1 = \mathbf{r}_{e1} - \mathbf{r}_{h1}, \tag{A2a}$$

$$\mathbf{r}_2 = \mathbf{r}_{e2} - \mathbf{r}_{h2}, \tag{A2b}$$

$$\mathbf{h} = \mathbf{r}_{h2} - \mathbf{r}_{h1}, \tag{A2c}$$

is the chosen set of relative coordinates and $\Phi(h)$ is the solution of the 2D interexciton Schrödinger equation (13). Inserting Eq. (A1) into Eq. (8) yields

$$F_a(s) = \frac{4\gamma^4}{\pi^2 2(1+S^2)}\int d\mathbf{r}_1 d\mathbf{r}_2 d\mathbf{h}\,\delta(\mathbf{r}_a - \mathbf{R} - \mathbf{s}) \times (e^{-2\gamma r_1}e^{-2\gamma r_2} + e^{-2\gamma|\mathbf{r}_1-\mathbf{h}|}e^{-2\gamma|\mathbf{r}_2+\mathbf{h}|} + 2e^{-\gamma r_1}e^{-\gamma r_2}e^{-\gamma|\mathbf{r}_1-\mathbf{h}|}e^{-\gamma|\mathbf{r}_2+\mathbf{h}|})\Phi^2(h) \quad (a = e1, e2, h1, h2), \tag{A3}$$

so that we finally receive for an electron

$$F_{ei}(s) = N\int_0^\infty dh\,h\Phi^2(h)[I_z(s,h) + J_{zz}(s,h)G(h)] \quad (i = 1,2), \tag{A4}$$

with

$$I_z(s,h) = \int_0^{2\pi} d\varphi_h e^{-2\gamma\sqrt{s^2+(h/2)^2+sh\cos(\varphi_h)}},$$

$$J_{zz}(s,h) = \int_0^{2\pi} d\varphi_h e^{-\gamma\sqrt{s^2+(h/2)^2+sh\cos(\varphi_h)}} \times e^{-\gamma\sqrt{s^2+(h/2)^2-sh\cos(\varphi_h)}},$$

$$G(h) = \frac{2}{\pi}\gamma^2\int_0^\infty dr\,re^{-\gamma r}\int_0^{2\pi} d\varphi_r e^{-\gamma\sqrt{r^2+h^2-2rh\cos(\varphi_r)}}, \tag{A5}$$

and for a hole

$$F_{hi}(s) = N\Phi(2s)[1 + I_{zz}^2(s)] \quad (i = 1,2), \tag{A6}$$

with

$$I_{zz}(s) = \frac{2}{\pi}\gamma^2\int_0^\infty dr\,re^{-\gamma r}\int_0^{2\pi} d\varphi_r e^{-\gamma\sqrt{r^2+4s^2+4rs\cos(\varphi_r)}}. \tag{A7}$$

$N$ is a normalization constant.

*Permanent address: Theoretical Applied Mechanics, Russian Academy of Science, Novosibirsk 630090, Russia.

[1] J. Ding, H. Jeon, T. Ishibara, M. Hagerott, A. V. Nurmikko, H. Luo, N. Samarth, and J. Furdyna, Phys. Rev. Lett. **69**, 1707 (1992); S. Chichibu, T. Azuhata, T. Sota, and S. Nakamura, Appl. Phys. Lett. **70**, 2822 (1997); A. Satake Y. Masumoto, T. Miyajima, T. Asatsuma, F. Nakamuva, and M. Ikeda, Phys. Rev. B **57**, R2041 (1998); P. Lefebvre, J. Allègre, B. Gil, A. Kavokine, H. Mathieu, W. Kim, A. Salvador, A. Botchkarev, and H. Moroç, , *ibid.* **57**, R9447 (1998); N. Grandjean, J. Massies, M. Leroux, and P. De Mierry, Appl. Phys. Lett. **72**, 3190 (1998); A. Vertikov, A. V. Nurmikko, K. Doverspike, G. Bulman, and J. Edmond, *ibid.* **73**, 493 (1998).

[2] L. Calcagnile, D. Cannoletta, R. Cingolani, M. Lomascolo, M. Di Dio, L. Vanzetti, L. Sorba, and A. Franciosi, Phys. Rev. B **55**, R13 413 (1997); L. Calcagnile, D. Greco, G. Coli', R. Cingolani, M. Lomascolo, M. Di Dio, L. Sorba, and A. Franciosi, Superlattices Microstruct. **21**, 119 (1997); G. Kuang, W. Gebhardt, E. Griebl, K. Jube, M. Kastner, M. Wörz, and T. Reisinger, Appl. Phys. Lett. **70**, 2717 (1997).

[3] J. Puls, H.-J. Wünsche, and F. Henneberger, Chem. Phys. **210**, 235 (1996).

[4] F. Kreller, M. Lowisch, J. Puls, and F. Henneberger, Phys. Rev. Lett. **75**, 2420 (1995); F. Kreller, J. Puls, and F. Henneberger, Appl. Phys. Lett. **69**, 2406 (1996); F. Kreller, H.-J. Wünsche, J. Puls, and F. Henneberger, J. Cryst. Growth **184/185**, 614 (1997).

[5] W. Langbein and J. M. Hvam, Phys. Status Solidi B **206**, 111 (1998).

[6] Y. Z. Hu, M. Lindberg, and S. W. Koch, Phys. Rev. B **42**, 1713 (1990).

[7] H.-J. Wünsche, S. Renisch, and F. Henneberger, Proc. SPIE **2994**, 102 (1997).

[8] R. Zimmermann, E. Runge, and F. Große, in *Proceedings of the 23rd ICPS 1996, Berlin*, edited by M. Scheffler and R. Zimmermann (World Scientific, Singapore, 1996), Vol. 3, p. 1935.

[9] V. A. Schweigert and F. M. Peeters, (unpublished); C. Riva, K. Varga, V. A. Schweigert, and F. M. Peeters (unpublished).

[10] Jia-Lin Zhu, Xi Chen, and Jia-Jiong Xiong, J. Phys.: Condens. Matter **3**, 9559 (1991).

[11] S. D. Baranowski, U. Doerr, P. Thomas, N. Naumov, and W. Gebhardt, Phys. Rev. B **48**, 17 149 (1993).
[12] Yang Wang, G. M. Stocks, W. A. Shelton, D. M. C. Nicholson, Z. Szotek, and W. M. Temmerman, Phys. Rev. Lett. **75**, 2867 (1995).
[13] J. R. Chelikovsky, N. Troullier, and Y. Saad, Phys. Rev. Lett. **72**, 1240 (1994).
[14] Rodney Price, Xuejun Zhu, S. DasSarma, and P. M. Platzman, Phys. Rev. B **51**, 2017 (1995).
[15] F. C. Zhang and S. DasSarma, Phys. Rev. B **33**, 2903 (1986).
[16] J. Singh, D. Birkedal, V. G. Lyssenko, and J. M. Hvam, Phys. Rev. B **53**, 15 909 (1996).
[17] I. A. Karp and S. A. Moskalenko, Fiz. Tek. Poluprovodn. **8**, 285 (1974) [Sov. Phys. Semicond. **8**, 183 (1974)].
[18] G. Otter and R. Honecker, *Atome-Moleküle-Kerne* (Teubner-Verlag, Stuttgart, 1996), Vol. II, p. 66.
[19] S. Flügge, *Rechenmethoden der Quantentheorie* (Springer-Verlag, Berlin, 1993), p. 279.
[20] In a more realistic treatment of the disorder potential (Ref. 21) it turns out that localization sites of axial symmetry occur with very low probability. While this has important consequences for the exciton fine structure and spin relaxation, the localization energy itself is not very sensitive on in-plane asymmetries of the potential justifying the use of Eq. (17) in the present context.
[21] H. Nickolaus, H.-J. Wünsche, and F. Henneberger, Phys. Rev. Lett. **81**, 2586 (1998).
[22] S. Glutsch, D. S. Chemla, and F. Bechstedt, Phys. Rev. B **54**, 11 592 (1996).
[23] L. D. Landau and E. M. Lifschitz, *Lehrbuch der Theoretischen Physik* (Akademie-Verlag, Berlin, 1986), Band III, Sec. 45.